

## Constitutive Relations for Modelling Macro Synthetic Fiber Reinforced Concrete

Humam Al-Sebai <sup>1</sup>, Zaid A. Al-Sadoon <sup>1\*</sup>, Salah Altoubat <sup>1</sup>, Mohamed Maalej <sup>1</sup>

<sup>1</sup> Department of Civil and Environmental Engineering, College of Engineering, University of Sharjah, United Arab Emirates.

Received 27 January 2024; Revised 26 April 2024; Accepted 08 May 2024; Published 01 June 2024

### Abstract

The increasing utilization of Fiber-Reinforced Concrete (FRC) within the construction industry signifies a pivotal shift towards enhancing structural integrity and durability. Despite the predominant use of steel fibers, exploring macro synthetic fibers has gained momentum due to their potential to address critical challenges, such as workability reduction and corrosion resistance in FRC, without markedly affecting its structural performance. Among the forefronts of FRC research is developing an accurate constitutive model encompassing the diverse behavior of fibers, particularly synthetic ones. This discrepancy necessitates a distinct constitutive model for synthetic fibers to precisely characterize their tensile post-cracking behavior and regulate their design specifications. In this research, a preliminary constitutive model is derived through an inverse analysis procedure employing a Generalized Reduced Gradient (GRG) optimization method to the load-displacement results of the experimental testing of twenty ASTM C1609 beam samples. The results of the inverse analysis are used to correlate the ASTM C1609 residual flexural tensile strength parameters,  $f_{L/600}$  and  $f_{L/150}$  to the stress-strain points defining the uniaxial tensile curve of macro-synthetic fibers, achieving coefficients of determination exceeding 98.5%. The model is statistically confirmed to be a valid constitutive relation for macro-synthetic fibers via successfully representing the post-cracking load-deflection behavior of standardized concrete beams, thereby outperforming traditional constitutive models in simulating the post-cracking behavior of FRC. Moreover, the model demonstrates robust predictive capabilities for the load-deflection curve of externally standardized samples, showcasing its potential for broader application in FRC design and analysis.

**Keywords:** Fiber Reinforced Concrete; Inverse Analysis; Macro-Synthetic Fibers; Constitutive Model; Residual Stresses; Stress-Strain Relations; Flexural Tests; Concrete Damage Plasticity; Finite Element Analysis.

### 1. Introduction

Macro Synthetic Fiber reinforced concrete (FRC) has been increasingly used for various structural applications, including slab-on grades, bridge decks, highway pavements, tunnel linings, and applications requiring magnetic inert materials [1]. The use of macro synthetic fibers as reinforcement is generally intended to control temperature and shrinkage cracks and improve the overall durability of concrete [2]. Moreover, using fibers in cast-in-place structural concrete members lessens the severity of bar reinforcement congestions and reduces expected crack sizes due to fibers' ability to increase confinement and redistribute localized stresses [3].

Unlike steel fibers, synthetic fibers are made through a chemical process from synthesized polymers of small molecules, giving them distinguished properties from steel fibers, such as their tensile strength and modulus of elasticity, which will exhibit a different post-cracking behavior relative to steel fibers when incorporated in concrete. Hence, using synthetic fibers as structural reinforcement in concrete has recently attracted the attention of academic researchers and

\* Corresponding author: [zalsadoon@sharjah.ac.ae](mailto:zalsadoon@sharjah.ac.ae)

<http://dx.doi.org/10.28991/CEJ-2024-010-06-06>



© 2024 by the authors. Licensee C.E.J, Tehran, Iran. This article is an open access article distributed under the terms and conditions of the Creative Commons Attribution (CC-BY) license (<http://creativecommons.org/licenses/by/4.0/>).

industry manufacturers. Furthermore, provisions and guidelines dictating the reproduction of synthetic FRC, and investigating their behavior are gradually progressing as more developments are made to (1) synthetic FRC raw materials [4, 5], (2) specialized applications of synthetic FRC [6-8], (3) enhancement of synthetic FRC mechanical properties [9-11]. (4) developing numerical computerized models of synthetic FRC [12-15], and (5) arriving at constitutive relationships to model synthetic FRC [16-20].

Currently, the inclination towards developing constitutive relations for synthetic FRC is increasing rapidly since a reliable constitutive material model is needed to design synthetic FRC structures, as there is still a lack of provisions regarding the use of macro synthetic fibers as supplemental reinforcement to concrete [2]. In the existing literature, most constitutive models were primarily developed for steel FRC, such as the RILEM Scientific Committee 162 recommendations [21], the fib Model Code [22], the German code [23], the Italian guideline [24], and the Spanish code [25]. Specifically, the design of FRC is based on the stress-strain ( $\sigma$ - $\epsilon$ ) relations representing both uniaxial compression and tension behavior. For compression, the adopted stress-strain relation is assumed to be similar to that of conventional concrete. On the other hand, the tensile behavior is modeled through an effective stress-strain relation that considers the post-cracking characteristics of FRC. This stress-strain relation is derived based on the residual strength parameters typically measured by standard flexural testing, such as the notched test of RILEM with a three-point loading configuration [20] and the unnotched test of ASTM with a four-point loading configuration [26].

The mechanical feature distinguishing synthetic fibers from steel fibers is the frictional bond strength response with slippage distance. For steel fibers, the uniaxial tensile strength exhibits a minimal reduction after the initial cracking but gradually decays due to bonding slip-weakening behavior for steel fibers. On the contrary, the uniaxial tensile strength of synthetic fibers is characterized by a sudden drop in load capacity after first cracking. However, due to the slip-hardening behavior of synthetic fibers, a gradual increase in the load capacity after cracking is observed, leading to a second post-cracking peak after further straining. Several studies have reported such behavior [3, 17, 27, 28]. The latter study suggests that the material uniaxial tensile behavior for synthetic FRC is fundamentally different from that of steel FRC, which impacts the uniaxial tensile stress-strain relation needed for modeling and designing macro synthetic FRC.

Numerous research studies [29-32] have shown that the analysis and design of FRC elements are profoundly dependent on the material tensile residual strength parameters. These parameters dictate the shape of the constitutive model, which has undergone extensive research development. Early attempts opted for a uniform residual tensile stress [33]. Later, a bilinear model was adopted and proved to fit the experimental data more accurately [34]. Rilem and the fib model code adopt such bilinear post-cracking tensile stress-strain relation to design FRC structures. This relation, together with the uniaxial compressive stress-strain curve, is directly used in the FEM material models to carry out the simulation and design of various FRC components subjected to a variety of loading conditions.

While the above bilinear models proved to be suitable for steel FRC, for macro synthetic FRC, a trilinear uniaxial tension stress-strain curve appears to be more suitable for capturing the various stages of the post-cracking response as previously described. This is confirmed by Stephen et al. [16], which found that the bilinear model does not satisfactorily represent the hardening response of FRC and suggests adopting trilinear or tetralinear models to yield more reasonable results for FRCs with both softening and hardening flexural responses. Moreover, the choice of the tensile constitutive laws used in the model can lead to substantial discrepancies in the numerical results [19].

The present study aims to propose a constitutive model for the uniaxial tensile response of macro-synthetic fibers suitable for implementation in FEM modeling. The constitutive model is based on trilinear uniaxial tension stress-strain relations whose parameters are obtained using an inverse analysis procedure from stress-strain data. The parameters of the constitutive model are subsequently linked through statistical analysis to residual strength parameters obtained from the ASTM standard C1609. The proposed model is later used to simulate the flexural behavior of standard macro-synthetic fiber beams. The performances of the proposed model, as well as those existing in the literature, are evaluated and compared to experimental test data from flexural beam tests using FEM programs.

Presently, no correlation coefficients are defined to directly link ASTM residual flexural strengths parameters defined for beam types tested per ASTM C1609/C1609M and ASTM C1399/C1399M to any code-proposed constitutive model [35]. Consequently, the significance of the work done in this research lies in providing numerical data that would help researchers develop a constitutive model for synthetic fibers based on standard ASTM residual strength parameters. Furthermore, this research will draw insight into the fitness of constitutive models proposed by the RILEM TC 162-TDF (2003) [21] and MC2010 fib Model Code (2010) [22] for modeling synthetic fibers. FEM simulations using ABAQUS are conducted to replicate the experimental load-displacement curves using the CDP model to represent the material behavior of synthetic FRC. The results from the code constitutive models are compared to those obtained by the proposed trilinear model. The proposed model significantly improves in representing the experimental load-displacement curves compared to the numerical simulations of both the RILEM TC 162-TDF (2003) [21] and MC2010 fib Model Code 2010 [22]. Specifically, the post-cracking behavior is observed to be underestimated by the RILEM TC 162-TDF (2003) [21] material model and overestimated by the MC2010 fib Model, while the proposed trilinear model gives the closest results to the experimental data.

## 2. Proposed Constitutive Model for Macro Synthetic FRC

The proposed constitutive model for macro synthetic FRC is derived based on several key stress points designated to define a piecewise continuous uniaxial tensile stress-strain constitutive relationship, as shown schematically in Figure 1. These key stress points are identified analytically by applying an inverse analysis procedure to the experimental flexural load-displacement data obtained per ASTM C1609. Specifically, the stress and strain values corresponding to the key points are correlated to the modulus of rupture  $f_r$  and the ASTM C1609 residual flexural tensile strengths  $f_{L/600}$  and  $f_{L/150}$ .

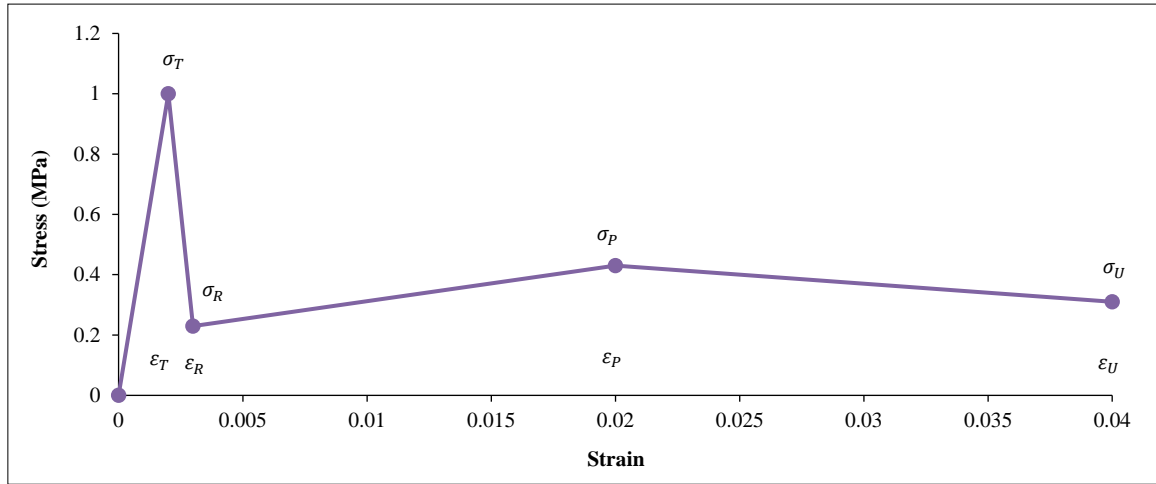


Figure 1. Schematic representation of the proposed trilinear constitutive model

The four key points specify the tensile stress-strain constitutive relationship, which defines a piecewise linearized post-cracking response of the FRC. The four key points are defined as follows:

- $\sigma_T$  and  $\varepsilon_T$ : The tensile strength corresponding to strain  $\varepsilon_T$
- $\sigma_R$  and  $\varepsilon_R$ : The residual tensile strength corresponding to strain  $\varepsilon_R$
- $\sigma_P$  and  $\varepsilon_P$ : The residual tensile strength corresponding to strain  $\varepsilon_P$
- $\sigma_U$  and  $\varepsilon_U$ : The residual tensile strength corresponding to strain  $\varepsilon_U$

### 2.1. Inverse Analysis

The applied inverse analysis method aims to determine synthetic FRC samples' tensile properties using the experimental data available from flexural tests. The inverse analysis procedure starts by dividing the cross-section into multiple thin layers, each of which is assumed to be subject to a constant strain. These strains are computed using the theory of simple bending, which relates the curvature to the strains. The curvature can be evaluated using the following expression, which is a function of the midpoint displacement [36]:

$$\varphi = \frac{2\delta(1-K)}{\delta^2(1-K)^2 + \left(\frac{L}{6}\right)^2} \quad (1)$$

The constant  $K$  is determined so that  $\varepsilon_{max} = \varepsilon_U = 0.4\%$  and is calculated by solving the following equation for  $K$ :

$$\frac{\varepsilon_{max}}{z-z_{NA}} \delta_{max}^2 K^2 - 2\delta_{max} \left(1 - \frac{\varepsilon_{max}}{z-z_{NA}} \delta_{max}\right) K + \frac{\varepsilon_{max}}{z-z_{NA}} \left(\delta_{max}^2 + \frac{L^2}{36}\right) - 2\delta_{max} = 0 \quad (2)$$

where  $L$  is the length of the sample between support points,  $\delta_{max}$  is the maximum deflection recorded in the load-displacement data log,  $z$  is the depth of the section, and  $z_{NA}$  is the depth of the N.A.

Subsequently, the curvature can be used to evaluate the strains at the centers of each layer of the cross-section according to the:

$$\varepsilon_c = \varphi(z - z_{NA}) \quad (3)$$

where  $z$  is the depth of the layer, while  $z_{NA}$  is the depth of the neutral axis. Assuming a linear distribution of the strain along the depth of the cross-section, as shown in Figure 2. The tensile stress distribution across the section is composed of a linear part in the elastic region and a nonlinear part in the post-cracking region. The linear part is defined as:

$$\sigma_t = E_c \varepsilon_t \quad , \quad \varepsilon_t \leq \varepsilon_{cr} \quad (4)$$

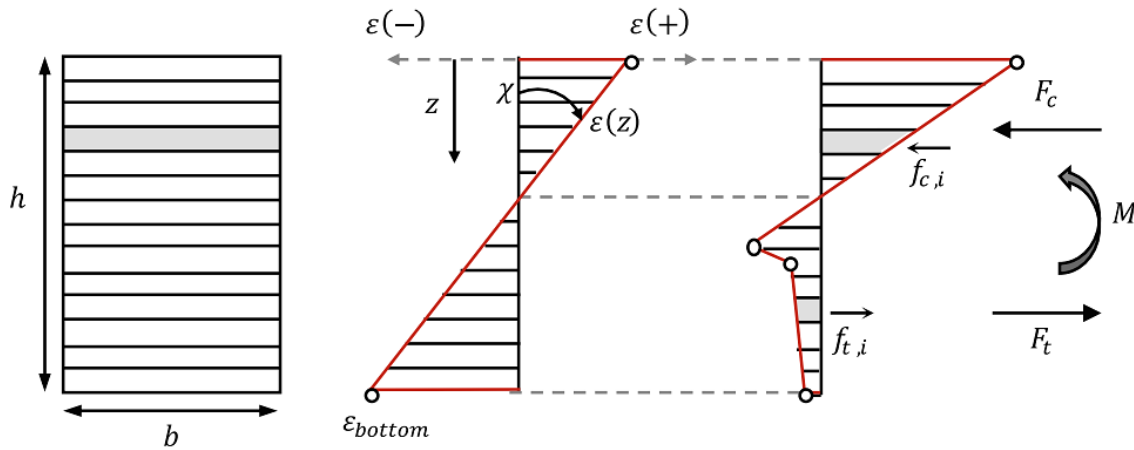


Figure 2. Distribution of strains and stresses across multilayered thin cross-sections

The nonlinear part of the stress function is evaluated using the Generalized Reduced Gradient GRG method. With the stress distribution thoroughly assessed, the force applied on each layer  $i$  is evaluated as:

$$F_i = (\sigma_{t,i} - \sigma_{c,i})bt = \sigma_i bt \tag{5}$$

Consequently, the net force of the section and the moment are evaluated as:

$$F = \sum F_i \tag{6}$$

$$M = \sum F_i(z - z_{NA}) \tag{7}$$

The value of  $M$  is calibrated to match the applied moment on the sample, which is;

$$M_p = \frac{PL}{6} \tag{8}$$

The flowchart in Figure 3 summarizes the inverse analysis procedure, which goes through an iterative process to evaluate the stress function. The linear part of the stress function is straightforward, but the nonlinear part of the relationship between the stress and the strain is found iteratively using the Generalized Reduced Gradient GRG method applied to the following equations.

$$\min_{z_{NA}, \sigma \in R^n} |F(z_{NA}, w(\varepsilon_t))| \tag{9}$$

$$\min_{z_{NA}, \sigma \in R^n} |M(z_{NA}, w(\varepsilon_t)) - M_p| \tag{10}$$

Subject to the following constraints:

- $0 < z_{NA} < H$
- $0 < \sigma$

where:

- $\varepsilon_t$  is the tensile strain
- $\varepsilon_{cr}$  is the cracking strain given as  $\frac{f_{ct}}{E_c}$
- $f_t$  is the tensile strength of concrete
- $E_c$  is the modulus of elasticity of concrete
- $w(\varepsilon_t)$  is the stress function
- $M_p$  is the applied moment on the beam

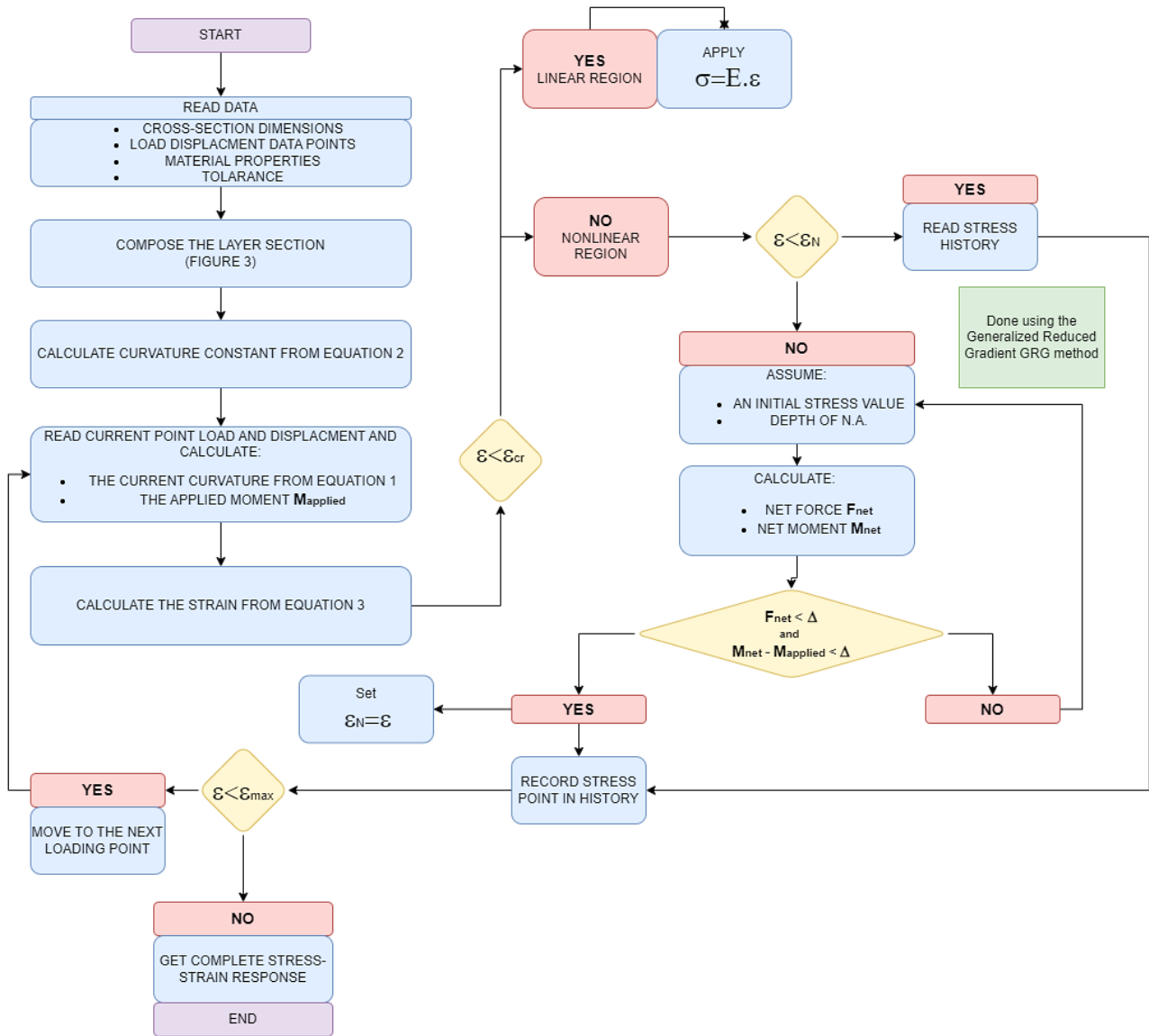


Figure 3. Flowchart of the inverse technique application process

The results of the GRG method are recorded and stored to be used for subsequent loading points. The maximum strain,  $\epsilon_N$ , for the stress history record is continuously updated. Thus, for each loading point, the curvature is evaluated from the displacement, and the strain is therefore calculated for the entire cross-section. The nonlinear part of the stress function developing over the cross-section is read from the stress history of the inverse analysis up to  $\epsilon_N$ . Beyond  $\epsilon_N$ , the GRG method is applied again, and the results are added to the stress history. This process is conducted at different stages of loading for the specimen and is repeated till the end of the available experimental data for each sample.

**2.2. Results of Inverse Analysis**

An approximate stress-strain response is produced for each sample using the results of the inverse analysis. Based on a process of MMSE regression, all the obtained stress-strain curves are appropriately linearized, and their endpoints are marked to be the key stress-strain points of the constitutive model. Figure 4 depicts the trilinear relations obtained along with the inverse analysis stress-strain relations of the samples. These trilinear stress-strain relations are defined in terms of four key points:  $\sigma_T$ ,  $\sigma_R$ ,  $\sigma_p$ , and  $\sigma_U$ , from the least to the highest strain, respectively. Table 1 displays the values obtained for these points.

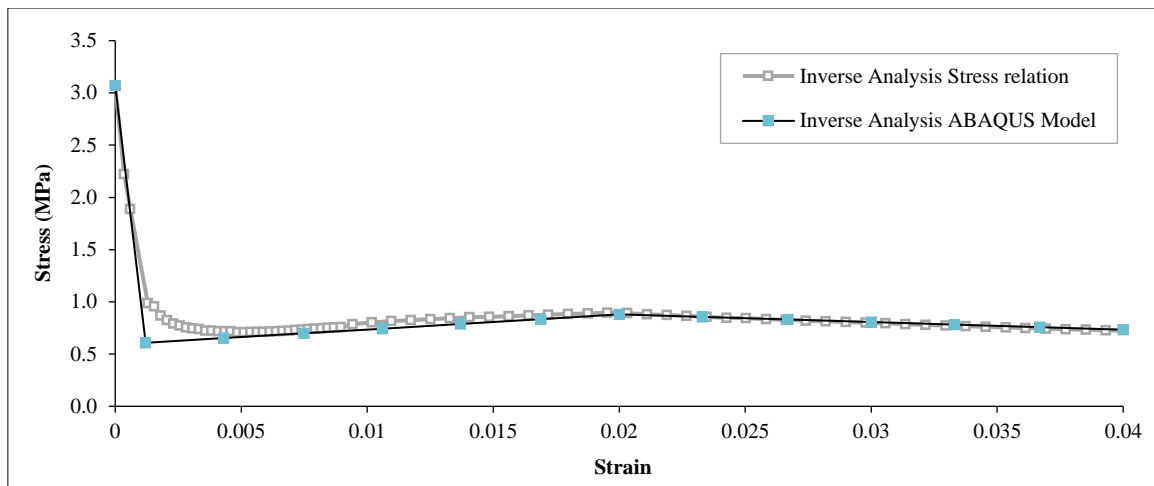


Figure 4. Trilinear relations obtained using MMSE regression

Table 1. Derivation of stress-strain values through MMSE linearization via inverse analysis

Samples	$\epsilon_T$	$\sigma_T$	$\epsilon_R$	$\sigma_R$	$\sigma_P$	$\sigma_U$
S1	0.000121	3.23	0.001857	0.36	0.57	0.31
S2	0.000117	2.4	0.001434	0.51	0.77	0.4
S3	0.000123	2.6	0.001273	0.59	0.98	0.52
S4	0.000123	2.63	0.003069	0.67	0.9	0.67
S5	0.000132	2.52	0.002	0.87	1.26	0.86
S6	0.000115	2.9	0.00206	0.71	0.94	0.68
S7	0.000121	3.58	0.001218	0.96	1.57	0.75
S8	0.000118	3.08	0.001805	0.96	1.67	0.78
S9	0.000113	3.25	0.001478	0.82	1.45	0.9
S10	0.000117	2.89	0.001301	0.32	0.38	0.25
S11	0.000136	2.08	0.001197	0.2	0.4	0.24
S12	0.000105	2.55	0.001445	0.31	0.37	0.24
S13	0.000119	2.83	0.00117	0.28	0.64	0.46
S14	0.000116	3.17	0.001195	0.47	0.65	0.52
S15	0.000127	2.84	0.002552	0.6	1.02	0.82
S16	0.000123	2.64	0.001822	0.46	0.65	0.44
S17	0.000128	2.9	0.001729	0.62	1.25	0.93
S18	0.000145	1.95	0.0029	0.49	0.55	0.35
S19	0.000130	2.71	0.003263	0.49	0.58	0.34
S20	0.000124	2.5	0.001783	0.37	0.51	0.33

### 2.3. Flexural Testing of FRC Samples

The ASTM C1609 is applied as a four-point beam test to 20 samples of the standard size (150 mm × 150 mm × 500 mm), as shown in Figure 5. The distance between the roller supports is specified to be 450 mm, and the distance between the two loading rollers is 150 mm. Based on these recommended standards, ASTM C1609 is chosen to evaluate the flexural performance of FRC because of the simplicity of test setup, test procedure, and support fixtures, in addition to the use of a closed-loop system which can self-correct based on feedback from the actuator displacement. The testing is conducted via a deformation-controlled loading that is applied at a rate of 0.05 mm per minute. Once the actuator deflection reaches 0.5 mm, the loading rate is increased to 0.25 mm per minute following the ASTM C1609 Standards. The mid-span deflection is measured via two linear variable differential transducers (LVDTs) clamped to both sides of the specimen, measuring the deflection at the top with a precision of ±0.001 mm. The average value of the two LVDTs is reported as the midspan net deflection of the specimen. The ASTM C 1609/C standard test method for flexural performance of fiber-reinforced concrete (using a beam with third-point loading) specifies two residual strength parameters:  $f_{L/600}$  and  $f_{L/150}$  that are calculated from their corresponding residual loads  $P_{L/600}$  and  $P_{L/150}$ .



Figure 5. Testing of beam flexure according to ASTM C1609 standard specifications

The samples are identical except for the varied volumetric fiber content across three levels: 0.5%, 0.75%, and 1%. The intention behind adopting three different volumetric ratios is to ensure that the sought constitutive relations are invariant to the volumetric ratios of fibers and are only dependent on the residual strength parameters obtained via the ASTM C1609 testing procedure. Table 2 contains the volumetric fiber ratios and their corresponding quantities for the three levels of fibers.

Table 2. Volumetric fiber ratios and their corresponding quantities

Strux Mix	0.5% Strux		0.75% Strux		1.0% Strux	
	kg/m <sup>3</sup>	Amount (kg)	kg/m <sup>3</sup>	Amount (kg)	kg/m <sup>3</sup>	Amount (kg)
S.P*	1.520	0.070	1.520	0.070	1.950	0.090
Strux	4.600	0.212	6.900	0.318	9.200	0.425

\* S.P is short for superplasticizer

Thus, the experimental program requires the preparation of 20 standard samples with a consistent mix design that only differs in the volumetric ratio of fibers. As the study is mainly concerned with synthetic fibers, STRUX 90/40 SDS™ macro fibers. They are 65 mm long, a diameter of 0.82 mm, an aspect ratio of 67, and a tensile strength of 585 MPa. Fibers are added to the mix design during the mixing stage to avoid having a potentially unrealistic alignment of fibers. The aim is to obtain a more natural random distribution of fibers (horizontally, vertically, and diagonally) that better reflects the properties of an actual FRC concrete member. The concrete matrix is produced using OPC. The concrete used had a 25 cm slump and had a w/b-ratio of 0.5. Additionally, nine cylindrical concrete samples were cast to determine the used FRC's compressive strength 24 hours after casting. The average compressive strength obtained was 27.8 MPa.

#### 2.4. Data Analysis of FRC Samples

Important material parameters, like the cracking strength of each sample, are calculated from the experimental data resulting from the C1609 ASTM testing procedure. Furthermore, the corresponding loads for the  $\frac{L}{600}$  and  $\frac{L}{150}$  displacements are recorded in addition to the least post-cracking load (LPCL), which is correspondingly used to obtain the LPCS, i.e., the least post-cracking strength. Likewise, these results are tabulated in Table 3 in addition to displacement at cracking load and the cracking strength. The Modulus of Rupture, in addition to the  $f_{L/600}$ , and the  $f_{L/150}$  residual strength is the correlation basis for the key points that define the proposed constitutive model. This is vital so the constitutive model is easily generated.

#### 2.5. Calibration of Constitutive Model

Using a linear regression model, the key stress points obtained correlate to their corresponding material testing parameter. Intuitively, the most natural choice is to correlate  $\sigma_T$  to the modulus of rupture,  $\sigma_R$  to the LPCS,  $\sigma_P$  to  $f_{L/600}$  and  $\sigma_U$  to  $f_{L/150}$ . Three out of these four parameters are considered standard parameters. Thus, only the LPCS parameter must be replaced with the most compatible standard material parameter. Upon inspection via scatter plot regression, it is found that  $f_{L/600}$  is closely correlated to the LPCS. This correlation is depicted in Figures 6 and 7.

**Table 3. Important sample test findings that describe the sample strength during and after cracking**

Samples	Displacement at Cracking Load (mm)	Cracking Strength MOR (MPa)	Displacement at LPCS (mm)	LPCS (MPa)	$f_{L/600}$ (MPa)	$f_{L/150}$ (MPa)
S1	0.05	4.89	0.19	1.60	2.01	1.32
S2	0.04	3.77	0.23	2.03	2.52	1.66
S3	0.05	3.86	0.16	2.32	3.13	2.06
S4	0.05	4.62	0.31	2.35	2.80	2.58
S5	0.05	4.82	0.18	2.91	3.79	3.23
S6	0.04	3.76	0.31	2.35	2.88	2.61
S7	0.05	5.43	0.12	3.19	4.53	2.87
S8	0.04	4.77	0.16	3.29	4.48	2.96
S9	0.04	4.44	0.11	2.78	4.16	3.36
S10	0.04	4.10	0.50	1.19	1.25	1.09
S11	0.05	3.66	0.50	1.32	1.34	1.07
S12	0.04	3.22	0.50	1.21	1.20	1.04
S13	0.04	4.01	0.18	1.69	2.08	1.85
S14	0.04	4.44	0.28	1.92	2.12	2.06
S15	0.05	4.50	0.22	2.26	2.93	3.08
S16	0.05	4.08	0.24	1.84	2.19	1.80
S17	0.05	4.78	0.15	2.37	3.37	3.46
S18	0.05	3.41	0.29	1.62	1.83	1.39
S19	0.05	4.45	0.26	2.02	2.29	1.90
S20	0.05	3.70	0.37	1.59	1.76	1.38

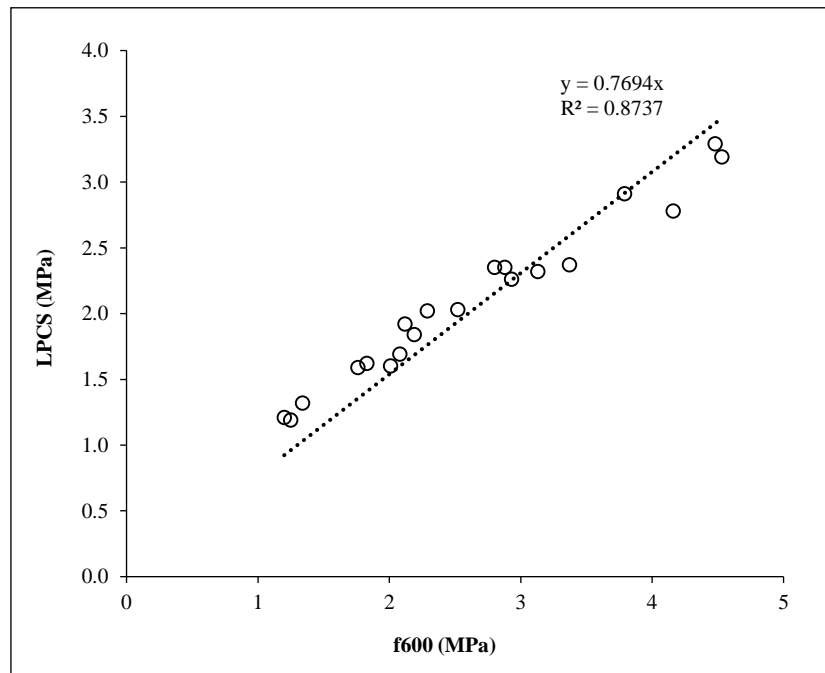


**Figure 6. Correlation analysis between samples LPCS and residual strength at f600 residual strength**

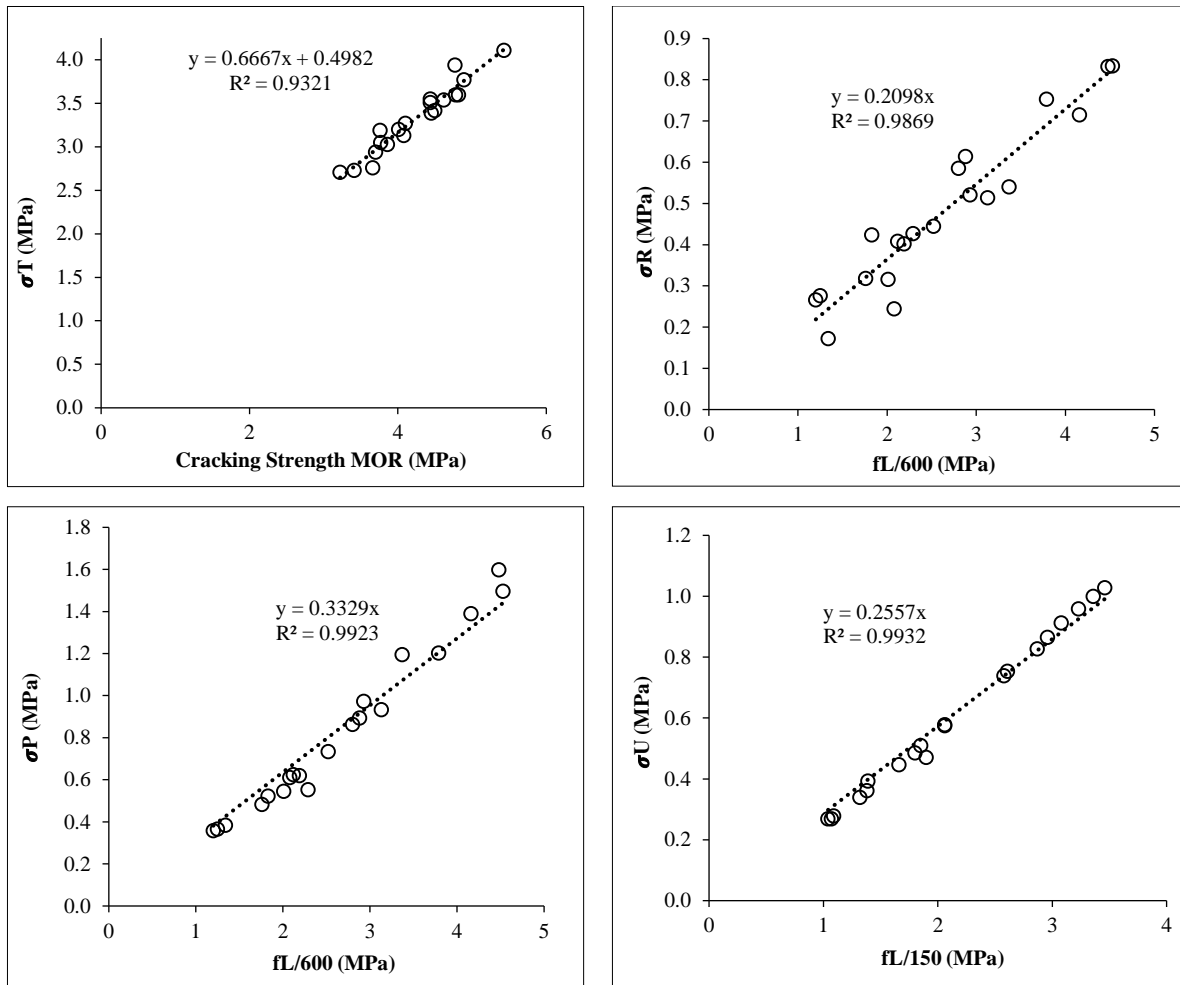


Figure 7. Correlations analysis between key points of the constitutive model versus MOR,  $f_{150}$ , and  $f_{600}$

### 2.6. Standardizing the Constitutive Model

As observed from Figures 6 and 7, all correlations are statistically strong, with coefficients of determination exceeding 98.5%. Substituting the proportionality factors of these correlations in the constitutive model yields a standardized constitutive model for synthetic FRC concrete material. The corresponding strains are defined according to their average values obtained from the inverse analysis. It is seen that,  $\sigma_p$  is reached in the proximity of 2% strain, while  $\epsilon_U$  varies significantly from 4% to 6%. By conducting sensitivity analysis, it is confirmed that this variation is of little significance to the resulting load-displacement simulated curve. As such, a value of 4% is chosen to be applied to all constitutive models. This choice is in agreement with Galeote et al. [28], who reported that extending the ultimate strain  $\epsilon_U$  up to 4% is necessary to reproduce a complete load-deflection curve fully. The results of the numerical models show that stresses defined for any strain level beyond  $\epsilon_U$  do not affect the results. This is attributed to the fact that the material fibers have already reached their bearing capacity at such strain levels. Numerically, this is reflected by a damage factor that is approaching unity. The value for  $\epsilon_T$  it can be determined strain forward from the ratio of  $\sigma_T$  to the modulus of elasticity  $E$ . Furthermore, the difference between  $\epsilon_T$  and  $\epsilon_R$  can be derived from the results of the inverse analysis procedure, which aligns with the value adopted by the fib model, i.e., 0.02%. The values of the stresses and the strains are illustrated in Table 4. Consequently, the standard trilinear model proposed by this paper for macro-synthetic FRC is shown in Figure 8, with all of its stress points clearly defined.

Table 4. Strain values for the standard constitutive model

Point	Strain Values	Stress Values	Stress Value (Approximate)
1	$\epsilon_T = \frac{\sigma_T}{E}$	$\sigma_T = 0.67f_r + 0.5$	$\sigma_1 \approx \frac{2}{3}f_r + 0.5$
2	$\epsilon_R = 0.02\%$	$\sigma_R = 0.21 f_{L/600}$	$\sigma_R \approx \frac{1}{5}f_{L/600}$
3	$\epsilon_P = 2\%$	$\sigma_P = 0.33 f_{L/600}$	$\sigma_P \approx \frac{1}{3}f_{L/600}$
4	$\epsilon_U = 4\%$	$\sigma_U = 0.26 f_{L/150}$	$\sigma_R \approx \frac{1}{4}f_{L/150}$

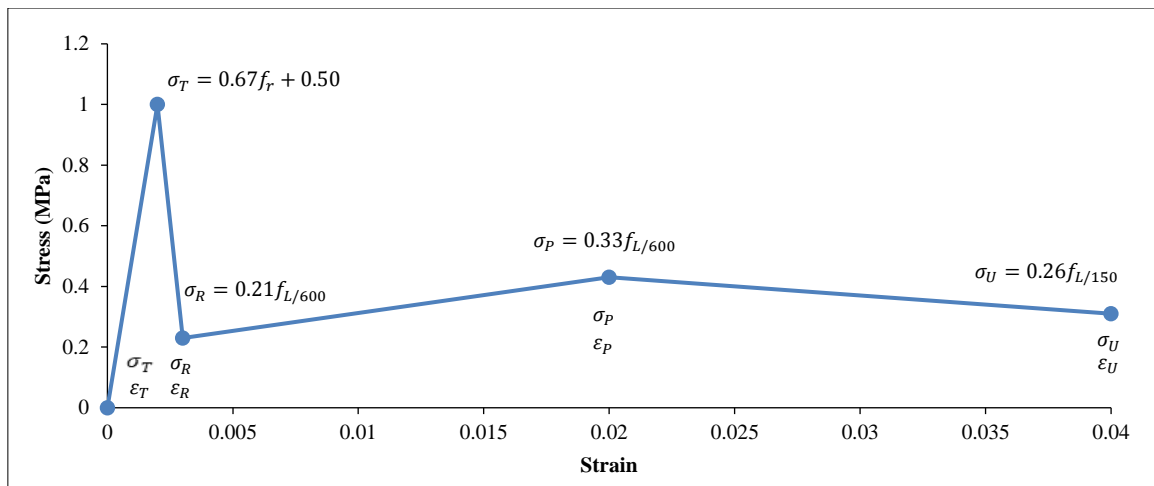


Figure 8. Standardized Constitutive Model for Macro-Synthetic Fiber-Reinforced Concrete

Following the relations obtained previously, each sample is marked by its unique constitutive model based solely on its standard ASTM material test parameters. Table 5 depicts the stress values for the key points of the standard constitutive model for all samples.

Table 5. Stress metrics at key points within the standard constitutive framework

Samples	$\sigma_T$	$\sigma_R$	$\sigma_P$	$\sigma_U$
S1	3.76	0.40	0.67	0.33
S2	3.01	0.50	0.84	0.42
S3	3.07	0.63	1.04	0.52
S4	3.58	0.56	0.93	0.65
S5	3.71	0.76	1.26	0.81
S6	3.01	0.58	0.96	0.65
S7	4.12	0.91	1.51	0.72
S8	3.68	0.90	1.49	0.74
S9	3.46	0.83	1.39	0.84
S10	3.23	0.25	0.42	0.27
S11	2.94	0.27	0.45	0.27
S12	2.65	0.24	0.40	0.26
S13	3.17	0.42	0.69	0.46
S14	3.46	0.42	0.71	0.52
S15	3.50	0.59	0.98	0.77
S16	3.22	0.44	0.73	0.45
S17	3.69	0.67	1.12	0.87
S18	2.77	0.37	0.61	0.35
S19	3.47	0.46	0.76	0.52
S20	2.97	0.35	0.59	0.35

### 3. Modelling of Flexural Tests

#### 3.1. Material CDP Model

Concrete, in general, is considered to have a complex material model. This fact is attributed to concrete's nonlinear stress-strain relationships, the dependence of the yielding function of concrete on multi-axial stress conditions, strain softening, anisotropic stiffness reduction, and progressive cracking caused by tensile stresses and strains [37]. Plasticity theory (along with fracture mechanics) plays a vital role in modeling concrete behavior when cracks are formed. Numerous researchers have focused their studies on achieving models that reflect and simulate the actuality of concrete behavior. Concrete Damage Plasticity (CDP) is one of the most efficient and successful elastoplastic models researchers commonly use to simulate concrete material. Despite its success, some inconveniences limit its usefulness, such as the need for defining uncoupled behavior along each principal stress (or strain) direction, the use of an entirely arbitrary

shear retention factor to ensure some shear resistance along the crack, and the lack of equilibrium at the cracking point when more than one crack is formed [38]. The stress-strain relation for a given concrete can be most accurately described based on uniaxial compression tests carried out on it. Following the work of Hsu & Hsu [39], a compressive stress-strain relation for uniaxial compression is defined as:

$$\sigma_c = \begin{cases} \sigma_{cu} \left( \frac{\lambda \beta \frac{\epsilon_c}{\epsilon_o}}{\lambda \beta - 1 + \left(\frac{\epsilon_c}{\epsilon_o}\right)^{\lambda \beta}} \right) & \lambda \beta \left(\frac{\epsilon_c}{\epsilon_o}\right) \left(\lambda \beta - 1 + \left(\frac{\epsilon_c}{\epsilon_o}\right)^{\lambda \beta}\right) \geq 0.6 \\ \sigma_{cu} \lambda \beta \left(\frac{\epsilon_c}{\epsilon_o}\right) \left(\lambda \beta - 1 + \left(\frac{\epsilon_c}{\epsilon_o}\right)^{\lambda \beta}\right) & \lambda \beta \left(\frac{\epsilon_c}{\epsilon_o}\right) \left(\lambda \beta - 1 + \left(\frac{\epsilon_c}{\epsilon_o}\right)^{\lambda \beta}\right) < 0.6 \end{cases} \quad (11)$$

where  $\lambda = 2$ ,  $\beta = \frac{1}{1 - \frac{\sigma_{cu}}{E_c \epsilon_o}}$ ,  $\epsilon_o = 8.9 \times 10^{-5} \sigma_{cu} + 2.114 \times 10^{-3}$ , and  $E_o = 1.243 \times 10^2 \sigma_{cu} + 3.28312 \times 10^3$ .  $\beta$  and  $\lambda$  are the material parameters.  $\beta$  depends on the shape of the stress-strain diagram;  $\lambda$  depends on the strength of the material. The tensile stress-strain curve applied in the analysis is derived from the proposed constitutive model. Figure 9 depicts the resulting stress distribution in a transverse section through the middle of the model, which characterizes the proposed trilinear model.

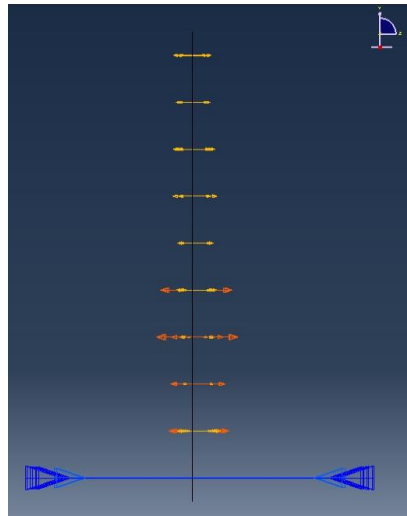


Figure 9. Stress distribution across a transverse section at the midpoint of the model

### 3.2. Abaqus Material Model

In ABAQUS, the model CDP is a continuum, plasticity-based damage model for concrete [40]. Abaqus CDP model features optional scalar stiffness degradation accumulation. The yield surface is given by a yield function incorporating a modified Drucker-Prager cone and Rankine tension cutoff. Isotropic strain hardening is defined with respect to two independent internal hardening variables, describing tensile and compressive behavior, respectively. The two hardening variables controlling the evolution of the yield (or failure) surface  $\tilde{\epsilon}_t^{pl}$  and  $\tilde{\epsilon}_c^{pl}$  are linked to failure mechanisms under tension and compression loading, respectively. The variables of the inelastic strains used in the CDP model are determined by obtaining a graph for a compression stress-strain relation. First, the elastic part, corresponding to the undamaged material, is deducted from the total strains registered in the uniaxial compression test. According to the CDP model, the plastic strain is given by the formula:

$$\tilde{\epsilon}_c^{pl} = \tilde{\epsilon}_c^{in} - \frac{d_c}{(1-d_c)} \frac{\sigma_c}{E_c} = \epsilon_c - \frac{1}{(1-d_c)} \frac{\sigma_c}{E_c} \quad (12)$$

$$\tilde{\epsilon}_t^{pl} = \tilde{\epsilon}_t^{ck} - \frac{d_t}{(1-d_t)} \frac{\sigma_t}{E_c} = \epsilon_t - \frac{1}{(1-d_t)} \frac{\sigma_t}{E_c} \quad (13)$$

where

- $\tilde{\epsilon}_c^{in} = \epsilon_c - \epsilon_{oc}^{el}$
- $\tilde{\epsilon}_t^{ck} = \epsilon_t - \epsilon_{oc}^{el}$
- $\epsilon_{oc}^{el} = \frac{\sigma_t}{E_c}$

It should be noted that plastic strain values can never be negative and/or decrease with increasing strains, which is typical for defining the damage variable. There is no consensus on the right way to define the damage variables other than the fact that it starts from zero at the strain corresponding to ultimate stress,  $\epsilon_o$ , and approaches a value of unity near the fracture point. In this research, the damage variables are related to the drop of the stress beyond  $\epsilon_o$ . In the

absence of tensile damage, it is assumed that  $\tilde{\varepsilon}_c^{pl} = \tilde{\varepsilon}_c^{in}$ . The damage factor  $d_t$ , is found similarly to the compression damage parameter. Plastic and stiffness recovery factors are used to describe the damage behavior of concrete under reciprocating loading, such as crushing, tensile cracking, crack closure, and stiffness recovery [41]. These factors are assumed based on experimental observation in most quasi-brittle materials, including concrete.

### 3.3. Samples Finite Element Modeling using ABAQUS

ABAQUS software was used to model and analyze the ASTM C1609 samples using a deformable 3D solid type of dimension  $150 \times 150 \times 500$  mm. The analysis is conducted by imposing displacement control deformation on the sample and simulating the actuator of the testing machine. The analysis mode is set to an implicit dynamic step in which the loading is recorded via the left and right reaction sets. The deformation is recorded via the sets subject to the displacement-imposed boundary condition. Based on the experimental results of the tested samples, their concrete material properties were estimated and listed in Table 6. The corresponding values for the compressive stresses and strains defined via equation 11 are shown in Table 7. The tensile stress-strain data obtained via the proposed constitutive model, as described in Figure 8, are listed in Table 8. The FEM developed in ABAQUS is meshed according to a sensitivity study undertaken to select the best mesh size based on the accuracy of the results. A size of 10 mm was deemed suitable for the analysis. This mesh is shown in Figure 10.

**Table 6. Material properties of concrete**

Concrete Properties	Value
Density (kg/m <sup>3</sup> )	2350
Young's modulus (N/mm <sup>2</sup> )	25600
Poisson Ratio	0.2

**Table 7. Compressive stress-strain data of concrete sample 1**

Compressive stress	Compressive strain
2.875	0
39.67	0.0009174
26.85	0.004093
13.16	0.007309
7.447	0.01017
4.497	0.01290
2.815	0.01557
1.806	0.01822
1.180	0.02085
0.7822	0.02346
0.5249	0.02608
0.3558	0.02868
0.2433	0.03129
0.1677	0.03389
0.1164	0.03649

**Table 8. Tensile stress-strain data of concrete sample 1**

Tensile stress	Tensile strain
3.880	0
0.321	0.0003
0.368	0.0036
0.415	0.0069
0.463	0.0102
0.51	0.0134
0.557	0.0167
0.604	0.0200
0.563	0.0233
0.522	0.0267
0.481	0.03
0.439	0.0333

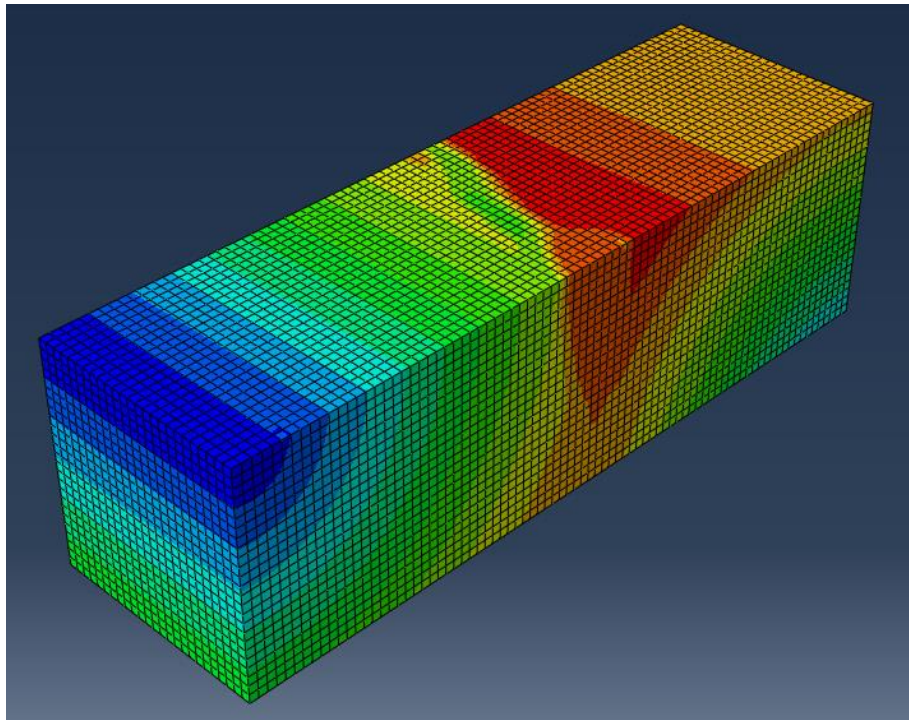
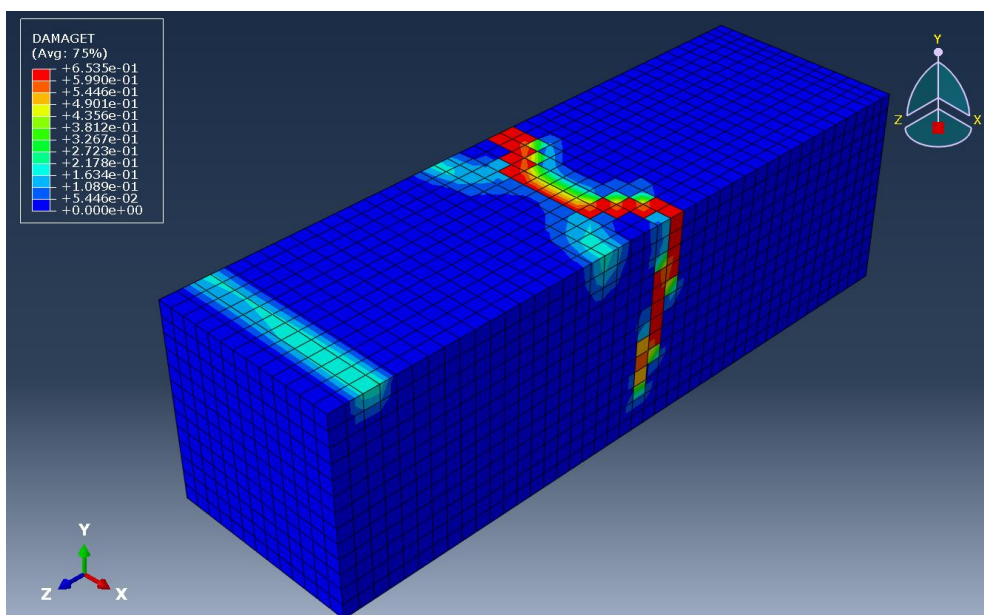


Figure 10. Finite element modeling of beam sample in Abaqus with a mesh size of 10 mm

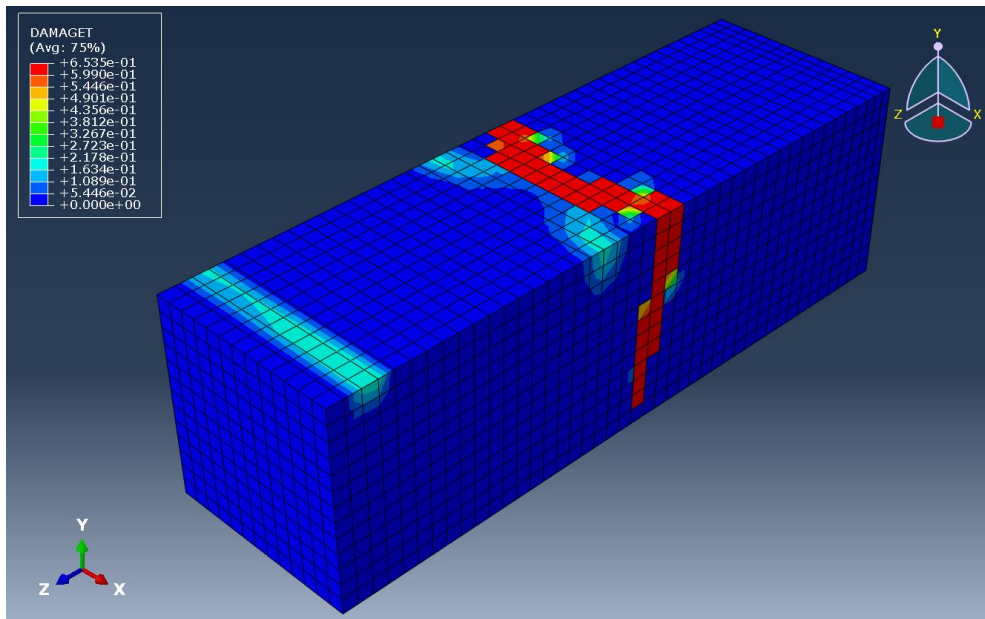
## 4. Results and Discussion

### 4.1. Validating the Constitutive Model

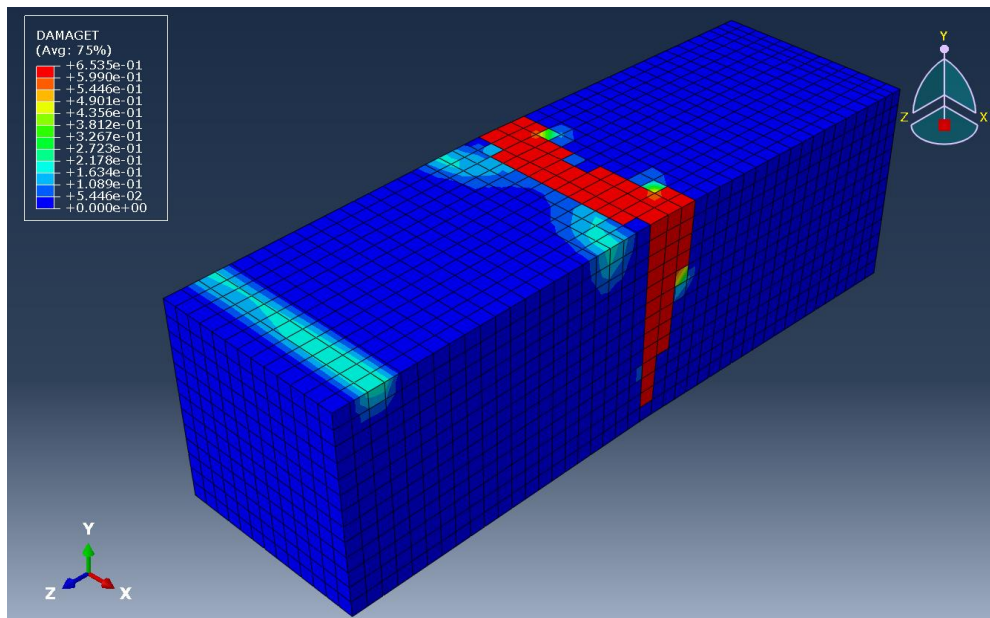
The corresponding parameters of the CDP model have been employed in ABAQUS. An implicit dynamic analysis is performed, and the test simulations are depicted via a deformation-controlled analysis mode. The boundary conditions in the FEM simulation are coincident with those applied in the ASTM C1609 beam test. Output is specified in two regions (left and right reactions). The load is the sum of the reactions at the support regions, while the displacement is the displacement of the two loading nodes corresponding to the loading pins that are applied to the sample. During the loading step, concrete damage due to tensile stresses occurs in the middle of the beam, signifying the occurrence of cracks in that area. Figure 11 displays the tension damage to the beam model during the loading step. Figure 12 depicts the plot of the original load-deflection curve for selected test samples alongside the implicit analysis modes of ABAQUS. Similar results were obtained for the rest of the 20 samples, which strongly suggest that the constitutive model has some potential to capture the behavior of synthetic fibers.



(a)

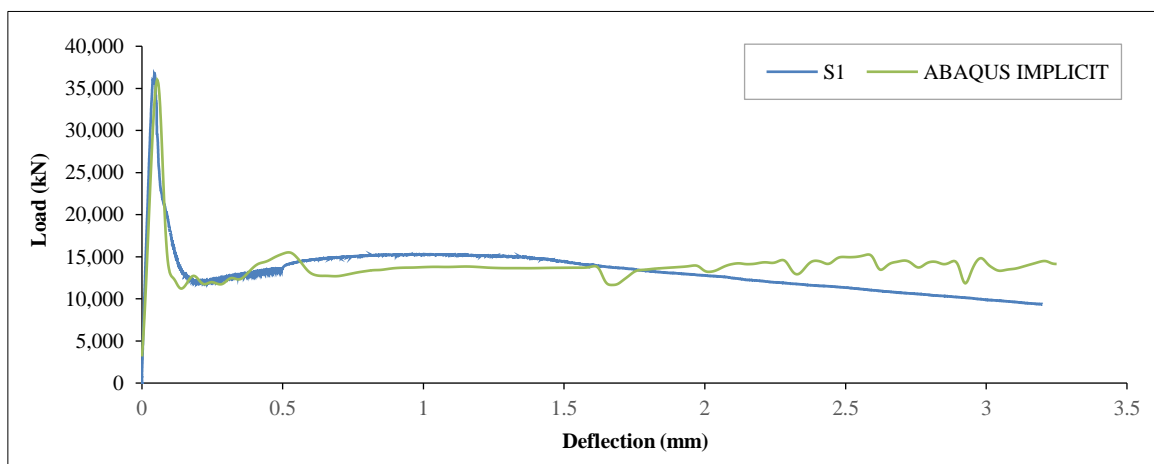


(b)



(c)

Figure 11. Tensile damage development in the beam FEM during the: (a) start, (b) middle, and (c) end of the loading step



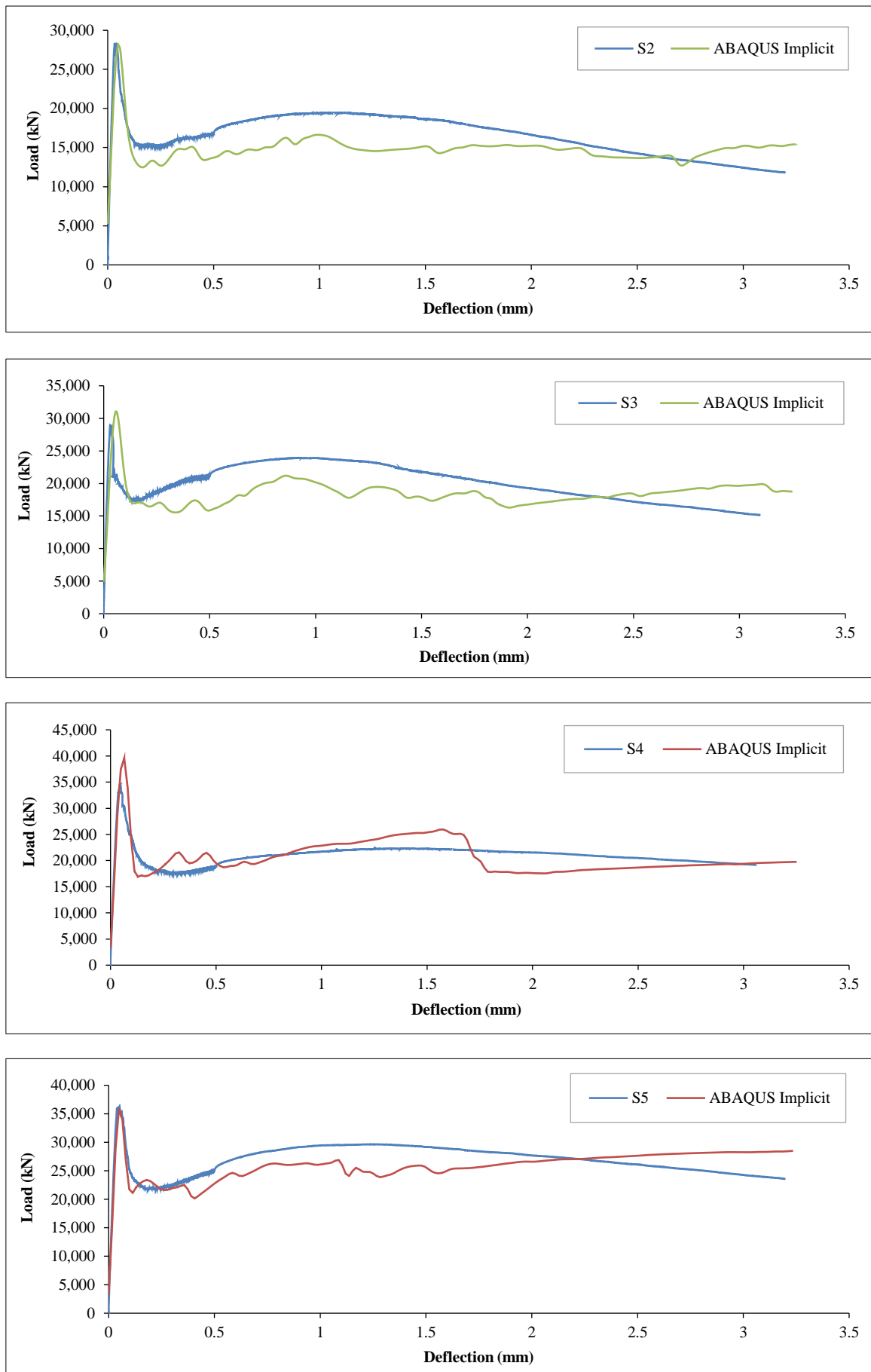


Figure 12. Comparative analysis of load-deflection curves: experimental results for the test samples versus ABAQUS implicit simulations

The load-displacement results shown in Figure 12 display good alignment between the experimental curve and the numerical analysis results. The numerical results capture the peak loading of the load-displacement curve, implying that the model can reasonably represent the material load-bearing capacity. The post-cracking response does not deviate much from the numerical simulation. Starting from the immediate strength loss after the peak point until the end of the failure, the overall shape of the numerical results is in agreement with the experimental results.

#### 4.2. Comparison with Existing Models

Most of the constitutive models for FRC in the literature are based on specific FRC constitutive laws that are adopted by codes and guidelines such as the RILEM Scientific Committee 162 recommendations [21], the fib Model Code [22], the German code [23], the Italian guideline [24], and the Spanish code [25]. Among these constitutive models, it is reported by Blanco et al. [42] that the constitutive models from the DBV, the RILEM, the EHE-08, and the fib Model MC2010 were the most accurate in representing the contribution of the fibers in the post-cracking. As a reference for comparison with the proposed model, the RILEM and the fib Model Code are considered. The Rilem and the fib constitutive models have been constructed for three samples following the specified procedures of both RILEM TC 162-TDF [21] and fib [22]. Tables 9 and 10 depict the stress-strain curves of the RILEM TC 162-TDF (2003) and MC2010 fib constitutive models obtained for three samples as inputted in ABAQUS, respectively.

**Table 9. Compilation of RILEM constitutive models for compatibility with the ABAQUS CDP framework**

Sample 1		Sample 2		Sample 3	
Stress (MPa)	Strain	Stress (MPa)	Strain	Stress (MPa)	Strain
6.330	0	5.640	0	5.820	0
0.78	0.0001	0.96	0.0001	1.21	0.0001
0.754	0.0022	0.929	0.0022	1.171	0.0022
0.728	0.0043	0.898	0.0043	1.132	0.0043
0.703	0.0063	0.868	0.0063	1.093	0.0063
0.677	0.0084	0.837	0.0084	1.053	0.0084
0.651	0.0105	0.806	0.0105	1.014	0.0105
0.625	0.0126	0.775	0.0126	0.975	0.0126
0.599	0.0146	0.744	0.0146	0.936	0.0146
0.573	0.0167	0.713	0.0167	0.897	0.0167
0.548	0.0188	0.683	0.0188	0.858	0.0188
0.522	0.0209	0.652	0.0209	0.818	0.0209
0.496	0.0229	0.621	0.0229	0.779	0.0229
0.47	0.025	0.59	0.025	0.74	0.025

**Table 10. Compilation of Fib constitutive models for compatibility with the ABAQUS CDP framework**

Sample 1		Sample 2		Sample 3	
Stress (MPa)	Strain	Stress (MPa)	Strain	Stress (MPa)	Strain
3.740	0	3.330	0	3.440	0
0.890	0.0002	1.070	0.0002	1.370	0.0002
0.87	0.001	1.05	0.001	1.34	0.001
0.85	0.0018	1.03	0.0018	1.31	0.0018
0.83	0.0025	1.01	0.0025	1.28	0.0025
0.81	0.0033	0.99	0.0033	1.25	0.0033
0.74	0.006	0.916	0.006	1.138	0.006
0.67	0.009	0.842	0.009	1.026	0.009
0.6	0.011	0.768	0.011	0.914	0.011
0.53	0.014	0.694	0.014	0.802	0.014
0.46	0.017	0.62	0.017	0.69	0.017

To depict how these models compare to each other, Figure 13 shows the constitutive models for (1) the proposed model, (2) RILEM TC 162-TDF (2003), and (3) MC2010 fib together side by side. Unlike Rilem and Fib, which are bilinear, the proposed model is trilinear. Figure 13 depicts the ABAQUS simulation's resulting load-deflection response for each constitutive model. It is clear from Figure 14 that Rilem underestimates the sample's post-cracking strength while the fib model overestimates it. The proposed constitutive model most accurately depicts the stress-strain response out of the three constitutive models. The results of Figure 14 are aligned with the findings of Galeote et al. [28], who followed a similar approach, conducting an inverse analysis procedure to determine the suitability of the fib MC2010 constitutive model to macro-synthetic fiber concrete incorporating polypropylene fibers as reinforcement. The results indicate that the MC2010 overestimates the residual strength of polypropylene fibers at small crack openings (SLS). Enfedaque et al. [3] reported similar results and concluded that the constitutive relations proposed by the MC2010 are above the experimental results.

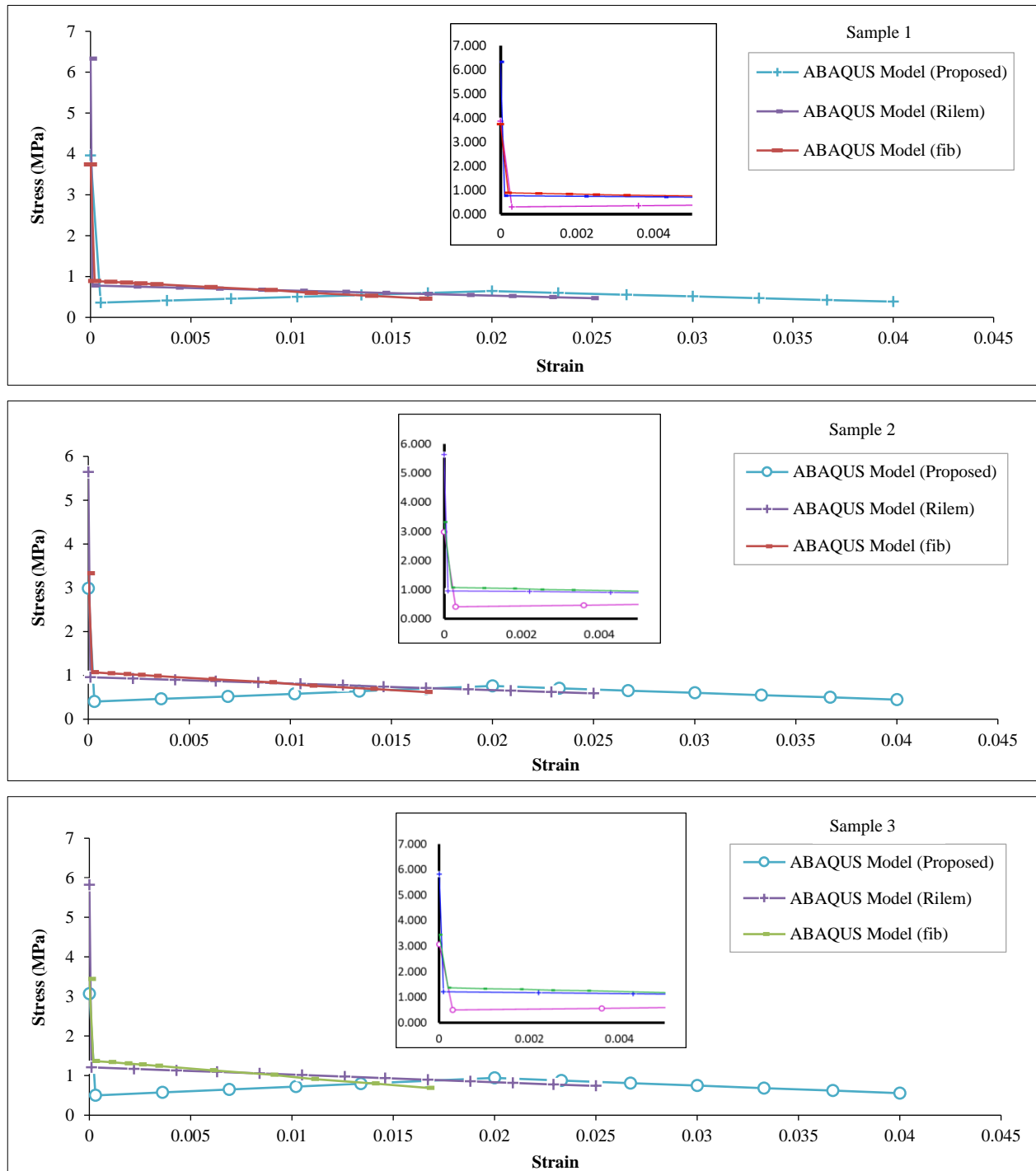
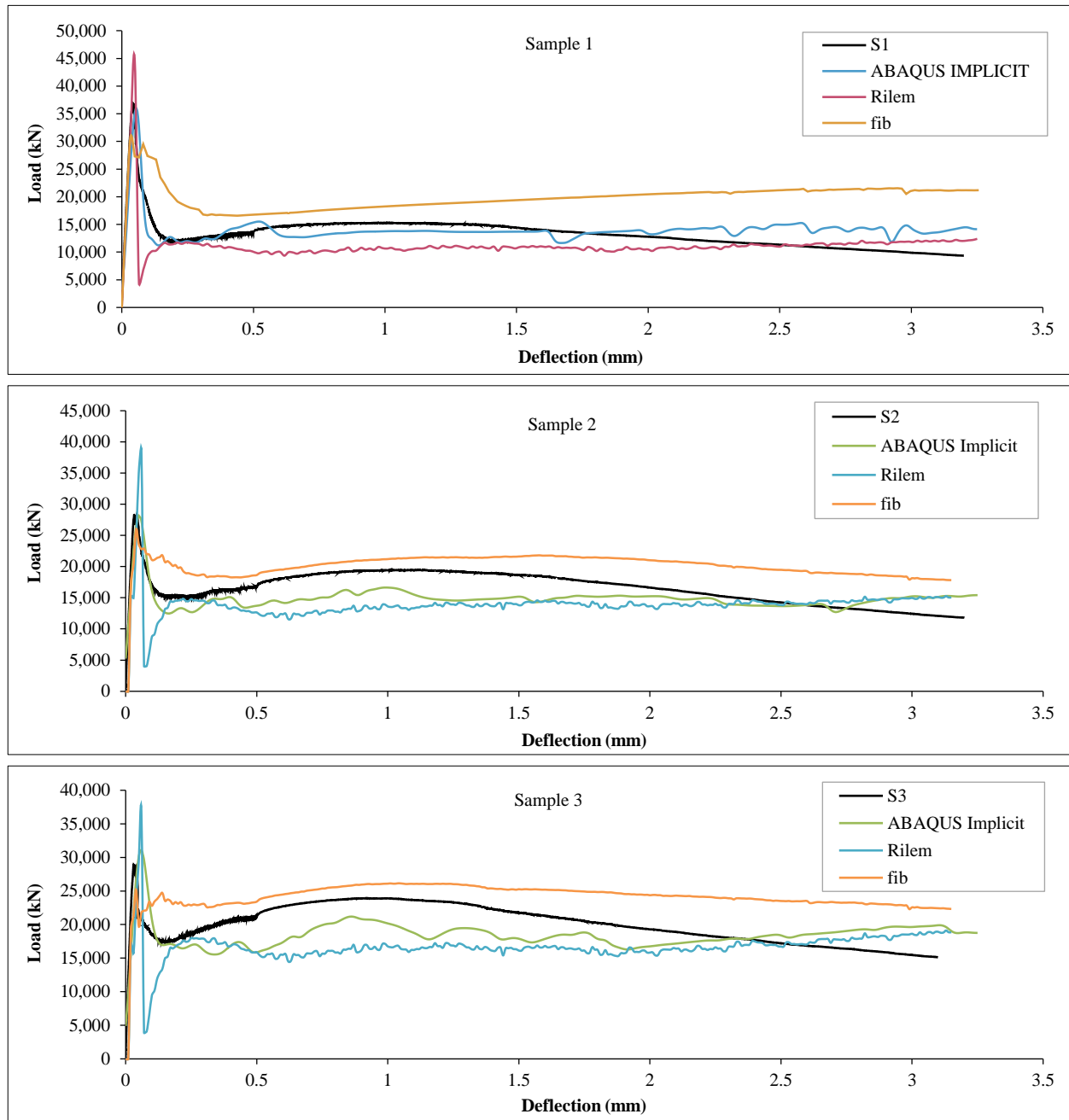


Figure 13. Comparison between the stress-strain curves of the proposed model versus Rilem and fib standards for the first three samples



**Figure 14. Comparison of constitutive models load-deflection of the three samples: Proposed model versus Rilem and fib standards**

As evident by the results shown in Figures 12 and 14, the proposed constitutive model adequately represents the material properties of macro-synthetic fibers under flexural testing. This can be verified by noticing the following:

1. Firstly, the stiffness of the numerical simulation agrees with that of the experimental results as the initial slope of the load-displacement curves match.
2. Secondly, the peak loading of the experimental load-displacement data agrees with the one predicted by the numerical results.
3. Thirdly, the overall shape of the post-cracking curve of the tested samples is reflected in the numerical model, and no major deviations are observed.

Thus, the proposed constitutive model has successfully linked the ASTM C1609 residual flexural tensile strength parameters,  $f_{600}$  and  $f_{150}$  in addition to modulating the modulus of rupture to the defining stress-strain points of the uniaxial tensile curve of macro-synthetic fibers. The results obtained via the proposed constitutive model surpass those obtained via conventional constitutive models such as the RILEM TC 162-TDF (2003) and the fib MC2010. This agrees with the findings of Stephen et al. [16] that bilinear models do not satisfactorily represent the hardening response of FRC. The study reported that trilinear models gave satisfactory results for FRCs with hardening flexural response and softening flexural response.

Three external samples have been selected from a research paper to further validate the suitability of the proposed constitutive model for modeling the behavior of macro synthetic FRC material [43]. The research study employed ASTM C1609 as a testing procedure to study the influence of hybridizing macro-size polyolefin and micro-size polypropylene fibers on concrete's fresh and hardened properties. The selected three samples contain only macro-synthetic fibers and are thus applicable for testing the constitutive model. The research study samples are made from the same mix design and share the properties shown in Table 11, while the volume fractions of the macro-synthetic fibers of the three samples are depicted in Table 12. The values of the ASTM parameters and the modulus of rupture of the three samples were used to generate the standard constitutive model for each sample. These models were fed into ABAQUS, and an explicit analysis of the results is shown in Figure 15 for samples M4, M7, and M10, respectively.

**Table 11. Proportional distribution of mixture samples**

Cement (kg/m <sup>3</sup> )	Water (kg/m <sup>3</sup> )	Sand (kg/m <sup>3</sup> )	Gravel (kg/m <sup>3</sup> )	HRWR (kg/m <sup>3</sup> )
90	164	877	965	1.17

**Table 12. Samples selected for constitutive model testing**

Sample Name	Macro Fiber Volume Fraction
M4	0.5
M7	1
M10	1.5

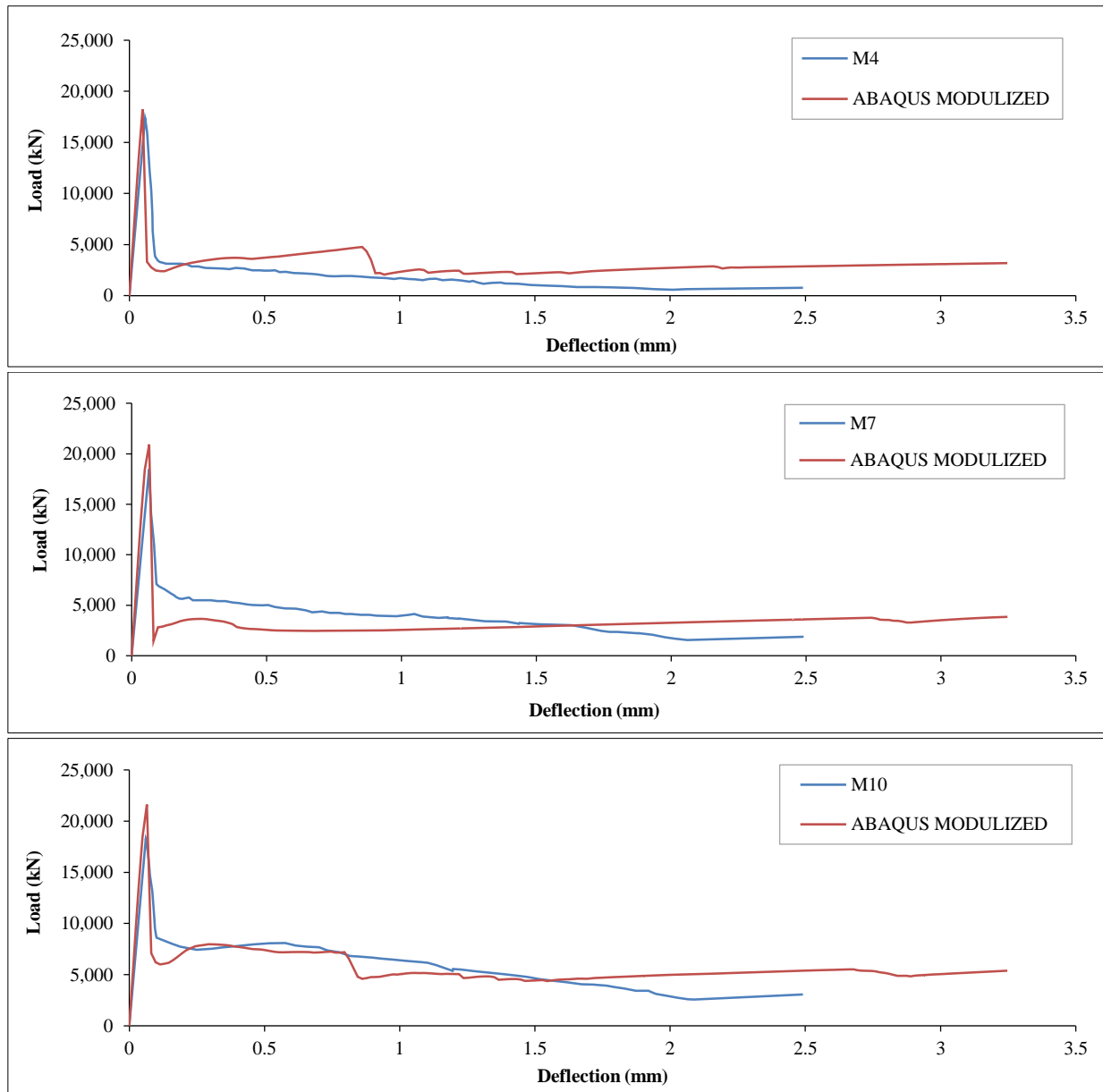


**Figure 15. Comparison between the load-deflection curves of the numerical simulations by the proposed model versus the results by Sadrinejad et al. [43]**

The results shown in Figure 15 further demonstrate that the proposed constitutive model accurately predicts the peak load and the post-cracking residual strength in all three samples with different volume fractions. The accuracy does not seem to be strongly influenced by the value of the volume fraction.

In summary, and based on the arguments mentioned above, the findings of this research suggest that the application of a trilinear constitutive model to represent the flexural behavior of macro-synthetic fibers is an improvement compared to conventional constitutive models that were generally developed based on sample results of steel FRC. Several studies by [3, 16, 27] have also reported similar conclusions, stating that the simulations carried out using a trilinear softening function showed a remarkable resemblance with the experimental behavior of synthetic FRC samples. Specifically, the peak load, the post-cracking response, and the unloading branch of the load-displacement curve were better replicated with higher accuracy using a trilinear constitutive model [3]. As a closing remark, it is important to note that the stress fields developed in real structures can deviate from the theoretical model due to many external effects, such as time-dependent phenomena, i.e., shrinkage and strength development over curing time. Further, simulation boundary conditions are ideal and rarely match the restraints in reality. Thus, the simulation output presented in this research must be generalized with caution.

## 5. Conclusions

Based on the discussed results related to the material modeling of macro synthetic FRC, it is possible to draw the following conclusions:

- The presented study significantly contributes to the Fiber-Reinforced Concrete (FRC) field by addressing the critical need for a constitutive model tailored to the unique characteristics of macro synthetic fibers. Through comprehensive Four-Point Bending Tests (4PBT) on beams following ASTM C1609 standards, this research has successfully introduced a preliminary constitutive model that embodies a notable advancement in accurately predicting the tensile post-cracking behavior of FRC.
- By employing an inverse analysis procedure, the study determined the stress-strain relationships for each beam sample. These relationships adhered to a trilinear stress-strain model, effectively depicting the post-cracking load-deflection characteristics of the concrete beams under standardized conditions. The model's validity was affirmed through a precise calibration process involving linear regression analyses between critical stress points derived from inverse analysis and the ASTM C1609 residual strength parameters. The robustness of the model is highlighted by a coefficient of determination greater than 98.5% and a standard deviation of the coefficients remaining below 2.5%, showcasing its efficacy in capturing peak loads and accurately reflecting the samples' post-cracking residual strength.
- The proposed constitutive model established a connection between the ASTM C1609 residual flexural tensile strength parameters,  $f_{600}$  and  $f_{150}$  and the stress-strain points defining the uniaxial tensile curve of macro-synthetic fibers. The results obtained via the proposed constitutive model surpass those obtained via code constitutive models such as RILEM TC 162-TDF (2003) and the fib MC2010.
- Comparative analyses underscore the model's superior precision in mirroring the load-deflection curves of beam samples over existing models such as RILEM and fib standards. Moreover, within Abaqus finite element (FE) simulations, it was perceived that implicit simulations offered enhanced accuracy over explicit simulations. The study further reveals the pivotal influence of mesh size on simulation accuracy, advocating for a 10 mm mesh size as optimal.
- The importance of this study extends to its potential implications for future research, particularly in developing stress coefficients that could align this new constitutive model with ASTM standards for macro-synthetic fibers in FRC. This is crucial as ASTM currently lacks a standardized stress-strain model for uniaxial tension in FRC, a gap that this research seeks to fill, marking a significant contribution to construction materials and engineering.

## 6. Declarations

### 6.1. Author Contributions

Conceptualization, H.S., Z.A., S.A., and M.M.; methodology, H.S., Z.A., M.M., and S.A.; software, H.S.; validation, M.M., S.A., Z.A., and H.S.; formal analysis, H.S., Z.A., S.A., and M.M.; investigation, H.S., M.M., S.A., and Z.A.; resources, S.A., M.M., and Z.A.; data curation, H.S.; writing—original draft preparation, H.S. and Z.A.; writing—review and editing, Z.A., M.M., and S.A.; visualization, H.S.; supervision, S.A., M.M., and Z.A.; project administration, S.A., M.A., and Z.A.; funding acquisition, S.A., M.M., and Z.A. All authors have read and agreed to the published version of the manuscript.

### 6.2. Data Availability Statement

The data presented in this study are available as an appendix in this article.

### 6.3. Funding

The authors received no financial support for the research, authorship, and/or publication of this article.

### 6.4. Conflicts of Interest

The authors declare no conflict of interest.

## 7. References

- [1] ACI PRC-506.1-08. (2008). Guide to Fiber-Reinforced Shotcrete. American Concrete Institute (ACI), Michigan, United States.
- [2] Thonstad, T, Calvi, P. (2023). Exploring the Combined Use of Distributed Fiber and Deformed Bar Reinforcement to Resist Shear Forces. University of Washington, Seattle, United States.
- [3] Enfedaque, A., Suárez, F., Alberti, M. G., & Gálvez, J. C. (2022). Suitability of Constitutive Models of the Structural Concrete Codes When Applied to Polyolefin Fibre Reinforced Concrete. *Materials*, 15(6), 2323. doi:10.3390/ma15062323.
- [4] Conforti, A., Tiberti, G., Plizzari, G. A., Caratelli, A., & Meda, A. (2017). Precast tunnel segments reinforced by macro-synthetic fibers. *Tunnelling and Underground Space Technology*, 63, 1–11. doi:10.1016/j.tust.2016.12.005.
- [5] Hou, J., Bai, J., Mou, H., & Xiang, Z. (2024). Tensile properties and constitutive model of cost-effective multiscale hybrid fiber reinforced strain hardening cementitious composites. *Frontiers in Materials*, 11. doi:10.3389/fmats.2024.1378089.
- [6] Lakavath, C., Suriya Prakash, S., & Dirar, S. (2021). Experimental and numerical studies on shear behaviour of macro-synthetic fibre reinforced prestressed concrete beams. *Construction and Building Materials*, 291, 123313. doi:10.1016/j.conbuildmat.2021.123313.
- [7] Zhao, J., Yang, X., Fan, J., Gao, S., & Ma, H. (2022). Research on Dynamic Compressive Performance of Polypropylene Fiber-Reinforced High-Strength Concrete under Freeze-Thaw Environment. *Advances in Materials Science and Engineering*, 2022, 1–12. doi:10.1155/2022/9079019.
- [8] Aidarov, S., Nogales, A., Reynvar, I., Tošić, N., & de la Fuente, A. (2022). Effects of Low Temperatures on Flexural Strength of Macro-Synthetic Fiber Reinforced Concrete: Experimental and Numerical Investigation. *Materials*, 15(3), 1153. doi:10.3390/ma15031153.
- [9] Buratti, N., Mazzotti, C., & Savoia, M. (2010). Experimental study on the flexural behaviour of fibre reinforced concretes strengthened with steel and macro-synthetic fibres. *Fracture Mechanics of Concrete and Concrete Structures-Assessment, Proceedings of FraMCoS-7, 23-28 May, 2010, Korean Concrete Institute, Seoul, South Korea.*
- [10] Huang, J., Zhang, Y., Tian, Y., Xiao, H., Shi, J., Shen, J., & Zhang, N. (2020). Research on the Dynamic Mechanical Properties and Constitutive Models of Steel Fiber Reinforced Concrete and Polypropylene Fiber Reinforced Concrete. *Advances in Civil Engineering*, 2020, 1–17. doi:10.1155/2020/9174692.
- [11] Zhang, Y., Ju, J. W., Zhu, H., Chen, Q., Guo, Q., & Yan, Z. (2019). A novel damage model based on micromechanics for hybrid fiber reinforced cementitious composites under uniaxial compression. *International Journal of Damage Mechanics*, 28(7), 1095–1132. doi:10.1177/1056789518813270.
- [12] Liang, N., Yan, R., Liu, X., Yang, P., & Zhong, Z. (2020). A Study of Impact Response and Its Numerical Study of Hybrid Polypropylene Fiber-Reinforced Concrete with Different Sizes. *Advances in Materials Science and Engineering*, 2020, 1–15. doi:10.1155/2020/6534080.
- [13] Carvalho, M. R., Barros, J. A. O., Zhang, Y., & Dias-da-Costa, D. (2020). A computational model for simulation of steel fibre reinforced concrete with explicit fibres and cracks. *Computer Methods in Applied Mechanics and Engineering*, 363. doi:10.1016/j.cma.2020.112879.
- [14] Bains, A. (2021). Numerical modelling of micro and macro cracking in plain and fibre-reinforced cementitious composites. Ph.D. Thesis, Cardiff University, Cardiff, Wales.
- [15] Dey, V., Bauchmoyer, J., Plesudjai, C., Schaefer, S., & Mobasher, B. (2021). Correlation of tensile and flexural response of continuous polypropylene fiber reinforced cement composites. American Concrete Institute, ACI Special Publication, SP-345, 230–242. doi:10.14359/51731584.
- [16] Stephen, S. J., Raphael, B., Gettu, R., & Jose, S. (2019). Determination of the tensile constitutive relations of fiber reinforced concrete using inverse analysis. *Construction and Building Materials*, 195, 405–414. doi:10.1016/j.conbuildmat.2018.11.014.
- [17] Zainal, S. M. I. S., Hejazi, F., Aziz, F. N. A. Abd., & Jaafar, M. S. (2020). Constitutive Modeling of New Synthetic Hybrid Fibers Reinforced Concrete from Experimental Testing in Uniaxial Compression and Tension. *Crystals*, 10(10), 885. doi:10.3390/cryst10100885.
- [18] Hashim, D. T., Hejazi, F., & Lei, V. Y. (2020). Simplified Constitutive and Damage Plasticity Models for UHPFRC with Different Types of Fiber. *International Journal of Concrete Structures and Materials*, 14(1), 45.
- [19] Zani, G., Martinelli, P., & di Prisco, M. (2022). Role of the tensile constitutive modeling on the structural response of fiber reinforced concrete flat slabs: A numerical study. *Structural Concrete*, 24(1), 1313–1327. Portico. doi:10.1002/suco.202200186.

- [20] ACI 544.8R-16. (2016). Report on indirect method to obtain stress-strain response of fiber-reinforced concrete (FRC). American Concrete Institute (ACI), Michigan, United States.
- [21] RILEM TC 162-TDF. (2003). Test and Design Methods for Steel Fiber Reinforced Concrete Sigma-Epsilon-Design Method. *Materials and Structures*, 36, 560-567.
- [22] MC2010 fib (2010). Mode Code 2010, Comité Euro-International du Béton-Federation International de la Précontrainte, Paris, France.
- [23] DBV. (2001). Information sheet on steel fibre concrete. Deutsche Beton Vereins, Berlin, Germany. (In German).
- [24] CNR-DT 204/2006. (2006). Instructions for the Design, Execution and Control of Fibre-reinforced Structures. Consiglio Nazionale delle Ricerche, Rome, Italy. (In Italian).
- [25] EHE-08. (2008). EHE-08 Structural Concrete Instruction. Comisión Permanente del Hormigón (Ministerio de Fomento), Spain. (In Spanish).
- [26] ASTM C1609/C1609M-19a. (2012). Standard Test Method for Flexural Performance of Fiber-Reinforced Concrete (Using Beam with Third-Point Loading). ASTM International, Pennsylvania, United States. doi:10.1520/C1609\_C1609M-19A.
- [27] Yang, L., Lin, X., Li, H., & Gravina, R. J. (2019). A new constitutive model for steel fibre reinforced concrete subjected to dynamic loads. *Composite Structures*, 221, 110849. doi:10.1016/j.compstruct.2019.04.021.
- [28] Galeote, E., Nogales, A., de la Fuente, A. (2023). Analysis of Design Constitutive Model for Macro-synthetic Fibre Reinforced Concrete Through Inverse Analysis. *Proceedings of the 75th RILEM Annual Week 2021, RW 2021, RILEM Book series*, 40, Springer, Cham, Switzerland. doi:10.1007/978-3-031-21735-7\_57.
- [29] Blazy, J., & Blazy, R. (2021). Polypropylene fiber reinforced concrete and its application in creating architectural forms of public spaces. *Case Studies in Construction Materials*, 14, e00549. doi:10.1016/j.cscm.2021.e00549.
- [30] Santos, L. C., Nogales Arroyo, A., Reginato, L., & Peralisi, R. (2020). Inverse analysis of constitutive models applied to steel fiber reinforced concrete. *Proceedings of the Ibero-Latin-American Congress on Computational Methods in Engineering: XLI CILAMCE: 16-19 November, 2020, Foz Do Iguacu Parana, Brazil*.
- [31] Lee, S. C., Cho, J. Y., & Vecchio, F. J. (2016). Analysis of steel fiber-reinforced concrete elements subjected to shear. *ACI Structural Journal*, 113(2), 275–285. doi:10.14359/51688474.
- [32] Ruiz, G., de la Rosa, Á., Wolf, S., & Poveda, E. (2018). Model for the compressive stress–strain relationship of steel fiber-reinforced concrete for non-linear structural analysis. *Hormigón y Acero*. doi:10.1016/j.hya.2018.10.001.
- [33] Guo, Y.-Q., Wang, J.-Y., & Gu, J.-B. (2022). Nonlinear Inverse Analysis for Predicting the Tensile Properties of Strain-Softening and Strain-Hardening UHPFRC. *Materials*, 15(9), 3067. doi:10.3390/ma15093067.
- [34] Lim, T. Y., Paramasivam, P., & Lee, S. L. (1987). Bending Behavior of Steel-Fiber Concrete Beams. *ACI Structural Journal*, 84(6), 524–536. doi:10.14359/2794.
- [35] Barros, J. A. O., & Figueiras, J. A. (1999). Flexural Behavior of SFRC: Testing and Modeling. *Journal of Materials in Civil Engineering*, 11(4), 331–339. doi:10.1061/(asce)0899-1561(1999)11:4(331).
- [36] Joshi, S., Paul, S., Balakrishnan, B., & Menon, D. (2015). Moment curvature relation of reinforced concrete T-beam sections: Numerical and experimental studies. *Third International Conference on Advances in Civil, Structural and Construction Engineering*, 10-11 December, Rome, Italy.
- [37] Hodhod, O. A., Sanad, A. M., El-Attar, M. M., & Hassan, H. A. (2019). Three-Dimensional Non-Linear Analysis of Two-Span Reinforced Concrete Beam-Using the Finite Element Code ABAQUS. *Al-Azhar University Civil Engineering Research Magazine (CERM)*, 41(1), 186-196.
- [38] Lubliner, J., Oliver, J., Oller, S., & Oñate, E. (1989). A plastic-damage model for concrete. *International Journal of Solids and Structures*, 25(3), 299–326. doi:10.1016/0020-7683(89)90050-4.
- [39] Hsu, L. S., & Hsu, C. T. T. (1994). Stress-strain behavior of steel-fiber high-strength concrete under compression. *ACI Structural Journal*, 91(4), 448–457. doi:10.14359/4152.
- [40] ABAQUS. (2014) Analysis User's Manual, Version 6.14. Dassault Systemes Simulia Inc., Johnston, United States.
- [41] Wang, Q., Hou, K. K., Lu, J., Dong, Q. H., Yao, D. P., & Lu, Z. (2020). Study on concrete damaged plasticity model for simulating the hysteretic behavior of RC shear wall. *IOP Conference Series: Materials Science and Engineering*, 789(1), 012065. doi:10.1088/1757-899x/789/1/012065.
- [42] Blanco, A., Pujadas, P., Cavalaro, S., de la Fuente, A., & Aguado, A. (2014). Constitutive model for fibre reinforced concrete based on the Barcelona test. *Cement and Concrete Composites*, 53, 327–340. doi:10.1016/j.cemconcomp.2014.07.017.
- [43] Sadrinejad, I., Madandoust, R., & Ranjbar, M. M. (2018). The mechanical and durability properties of concrete containing hybrid synthetic fibers. *Construction and Building Materials*, 178, 72–82. doi:10.1016/j.conbuildmat.2018.05.145.